

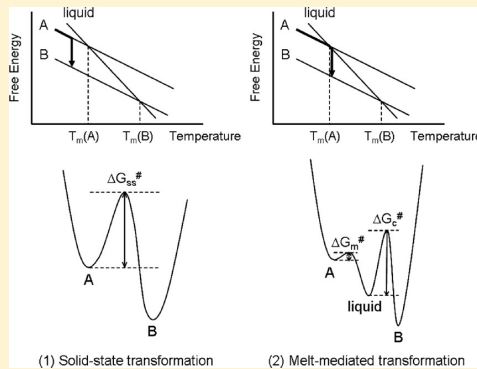
# Crystallization and Transformation of Polymorphic Forms of Trioleoyl Glycerol and 1,2-Dioleoyl-3-rac-linoleoyl Glycerol

Laura Bayés-García,<sup>\*,†</sup> Teresa Calvet,<sup>†</sup> Miquel Àngel Cuevas-Diarte,<sup>†</sup> Satoru Ueno,<sup>‡</sup> and Kiyotaka Sato<sup>‡</sup>

<sup>†</sup> Departament de Cristal·lografia, Mineralogia i Dipòsits Minerals, Facultat de Geologia, Universitat de Barcelona, Martí i Franquès s/n, E-08028 Barcelona, Spain

<sup>‡</sup> Faculty of Applied Biological Science, Hiroshima University, Higashi-Hiroshima 739, Japan

**ABSTRACT:** This study examined the influence of different thermal treatments on the crystallization and transformation of trioleoyl glycerol (OOO) and 1,2-dioleoyl-3-rac-linoleoyl glycerol (OOL). Two triacylglycerol (TAG) samples were cooled at  $0.5\text{--}15\text{ }^{\circ}\text{C}\cdot\text{min}^{-1}$  and heated at 2 and  $15\text{ }^{\circ}\text{C}\cdot\text{min}^{-1}$ . The polymorphic characteristics of the two TAGs were analyzed in situ using differential scanning calorimetry, Raman spectroscopy, and synchrotron radiation X-ray diffraction. Multiple polymorphic forms were identified in OOO ( $\alpha$ ,  $\beta'$ ,  $\beta'_1$ ,  $\beta_2$ , and  $\beta_1$ ) and OOL ( $\alpha$ ,  $\beta'_2$ , and  $\beta'_1$ ). Larger quantities of more stable forms (e.g.,  $\beta_2$  and  $\beta_1$  of OOO and  $\beta'_1$  of OOL) were obtained when the samples were slowly cooled and heated. In contrast, less stable polymorphs were obtained with increased cooling and heating rates. Polymorphic transformations occurred in either solid-state or melt-mediation and were influenced by heating rates. The results were analyzed by considering the activation energies for crystallization and transformation of stable and less stable polymorphic forms in comparison with previous studies on 1,3-dipalmitoyl-2-oleoyl-glycerol and 1,3-dioleoyl-2-palmitoyl-glycerol.



## INTRODUCTION

Lipids are major nutrients employed in the food, pharmaceutical, and cosmetic industries<sup>1</sup> as lipophilic materials. In this large group of compounds, triacylglycerols (TAGs) are the main components of natural and industrial fats and oils. The physical properties (e.g., melting, morphology, rheology, and texture<sup>2</sup>) of TAGs depend mainly on their fatty acid structures and compositions, which are most typically revealed in polymorphism. The complexity of polymorphism and the number of polymorphic forms of TAGs are strongly related to the chemical nature of the fatty acid components (chain length, saturated or unsaturated, cis or trans double bonds).<sup>1</sup>

Controlling the polymorphism of TAGs to obtain the desired product characteristics is an important challenge for the industrial fields (e.g., pharmaceutical, biomedical, and food). Therefore, many studies have addressed the influence of external factors on the polymorphic characteristics of TAGs (e.g., additives,<sup>3</sup> shear,<sup>4</sup> and sonication<sup>5</sup>).

The effects of temperature variation have also been studied, since the kinetic properties of polymorphic crystallization and transformation of TAGs are significantly influenced by the rates of cooling and heating of the TAG samples in neat liquid and emulsion states. This is because the influences of dynamic temperature variations are exhibited differently in metastable forms than in more stable polymorphic forms. Thus, many researchers have studied the influences of thermal treatments on the polymorphic behavior of TAGs, from pure TAGs<sup>6–8</sup> to more complex or natural samples.<sup>9–12</sup> Recently, we reported on the

effects of varied cooling rates on the polymorphic crystallization of 1,3-dioleoyl-2-palmitoyl glycerol (OPO),<sup>7</sup> and the effects of changing both cooling and heating rates on the crystallization and transformation pathways of 1,3-dipalmitoyl-2-oleoyl glycerol (POP)<sup>8</sup> using differential scanning calorimetry (DSC) and synchrotron radiation X-ray diffraction (SR-XRD) with small-angle X-ray diffraction (SAXD) and wide-angle X-ray diffraction (WAXD). SR-XRD and DSC provided highly accurate information and permitted in situ monitoring of the polymorphic crystallization and subsequent transformations, even if high cooling/heating rates (e.g.,  $15\text{ }^{\circ}\text{C}\cdot\text{min}^{-1}$ ) were applied.

This study reports on the polymorphic characteristics of trioleoyl-glycerol (OOO) and 1,2-dioleoyl-3-linoleoyl glycerol (OOL), which are the main triunsaturated TAGs present in vegetable oils (e.g., olive oil<sup>13</sup>) and other edible oils, by dry fractionation of palm oil.<sup>14</sup> The crystallization characteristics of these low-melting TAGs are important for the physical properties of foods employed at chilled temperatures (e.g., frozen foods).

Regarding the polymorphism of OOO, Wheeler et al.<sup>15</sup> demonstrated the existence of “three crystalline or solid forms: Form I, Form II, and Form III” and presented their melting point data. Later, Ferguson et al.<sup>16</sup> determined the long- and short-spacing values of three polymorphic forms of OOO:  $\alpha$ ,  $\beta'$ , and  $\beta$ .

Received: April 18, 2013

Revised: June 25, 2013

Published: July 10, 2013

More polymorphs were characterized by Hagemann et al.,<sup>17</sup> who reported that three  $\beta'$  forms ( $\beta'_1$ ,  $\beta'_2$ , and  $\beta'_3$ ) appeared when different thermal treatments were applied. They conducted DSC and IR experiments but provided no XRD data on the newly found  $\beta'$  forms. Sato and Ueno noted the presence of three  $\beta'$  forms and two  $\beta$  forms in OOO<sup>18</sup> but presented no details. Akita et al.<sup>19</sup> recently reported the molecular conformations and crystal structures of  $\alpha$ ,  $\beta'$ , and  $\beta$  forms using a combination of XRD, infrared (IR), and Raman methods. However, few studies have focused on the kinetic properties of the crystallization and transformation of polymorphic forms of OOO.

In this study, we applied DSC, SR-XRD, and micro-Raman methods to in situ observation of the crystallization and transformation kinetics of OOO and OOL. To avoid the effects of impurities on polymorphic characteristics, we used highly pure samples of OOO and OOL. Different thermal treatments were applied to the samples by changing the cooling and heating rates. Long- and short-spacing values were determined for all the studied polymorphic forms of OOO ( $\alpha$ ,  $\beta'_2$ ,  $\beta'_1$ ,  $\beta_2$ , and  $\beta_1$ ) and OOL ( $\alpha$ ,  $\beta'_2$ , and  $\beta'_1$ ). To the best of our knowledge, this study is the first to examine the polymorphic characteristics of OOL.

## MATERIALS AND METHODS

Samples of OOO and OOL were purchased from Tsukishima Foods Industry Co., Ltd. (Tokyo, Japan) and used without further purification. The sample purity was 99.4% (OOO) and 99.0% (OOL), analyzed using HPLC (private communication from Tsukishima Foods Industry Co., Ltd.).

DSC experiments were conducted at atmospheric pressure using both a Perkin-Elmer DSC-7 (for the shortest thermal treatments) and a Perkin-Elmer DSC Diamond (for the longest ones). The DSC thermograms obtained by the two calorimeters were comparable. Samples (9.0–9.4 mg) were weighed into 50  $\mu\text{L}$  aluminum pans, and covers were sealed into place. Both instruments were calibrated with reference to the enthalpy and the melting points of indium (melting temperature, 156.6 °C;  $\Delta H$ , 28.45 J/g) and decane (melting temperature, -29.7 °C;  $\Delta H$ , 202.1 J/g) standards. An empty pan was used as a reference. Dry nitrogen was used as the purge gas in the DSC cell (at 23 cm<sup>3</sup>/min in the Perkin-Elmer DSC-7 and at 20 cm<sup>3</sup>/min in the Perkin-Elmer DSC Diamond). Thermograms were analyzed with Pyris software to obtain the enthalpy (J/g, integration of the DSC signals) and  $T_{\text{onset}}$  of the transitions (°C, intersections of the baseline and the initial tangent at the transition).

Samples were subjected to different cooling and heating rates in the following patterns: OOO was cooled (15, 2, 1, and 0.5 °C·min<sup>-1</sup>), heated (15 °C·min<sup>-1</sup>), cooled (2 °C·min<sup>-1</sup>), and heated (2 °C·min<sup>-1</sup>). OOL was cooled (15 °C·min<sup>-1</sup>), heated (15 and 0.5 °C·min<sup>-1</sup>), cooled (2 °C·min<sup>-1</sup>), heated (2 °C·min<sup>-1</sup>), cooled (0.5 °C·min<sup>-1</sup>), and heated (15 °C·min<sup>-1</sup>). At least three independent measurements were made for each experiment ( $n = 3$ ). Random uncertainty was estimated with a 95% threshold of reliability using the Student's *t*-distribution, which enables estimation of the mean of a normally distributed population when it is small.<sup>20</sup> A correction (described elsewhere<sup>7</sup>) was applied for analyses with cooling or heating rates other than 2 °C·min<sup>-1</sup>, since both calorimeters were calibrated at this rate.

SR-XRD experiments were performed at two different beamlines (BL-15A and BL-9C) of the SR source Photon Factory (PF) of the High-Energy Accelerator Research Organization (KEK) in Tsukuba (Japan). For both beamlines, a double-focusing camera operated at a wavelength of 0.15 nm. In

BL-9C, the X-ray scattering data were simultaneously collected by position sensitive proportional counters (PSPCs) (Rigaku Co., PSPC-10), SAXD, and WAXD. In BL-15A, a camera with a charge-coupled device (CCD) was used for small-angle data, and a PSPC for wide-angle data. Each temperature program was controlled by a Mettler DSC-FP84 (Mettler Instrument Corp., Greifensee, Switzerland) with FP99 software. A 2-mm-thick sample was placed in an aluminum sample cell with Kapton film windows. SR-XRD spectra were acquired at 30 or 60 s intervals, depending on the cooling and heating rates used and the complexity of the thermal profile.

Conventional powder XRD was used for some intermediate cooling and heating rates using a PANalytical X'Pert Pro MPD powder diffractometer equipped with a Hybrid Monochromator and an X'Celerator Detector. The equipment also included an Oxford Cryostream Plus 220 V (temperature 80–500 K). This diffractometer operates with Debye–Scherrer transmission. The sample was introduced in a 1 mm-diameter Lindemann glass capillary that was rotated around its axis during the experiment to minimize preferential orientation of the crystallites. The step size was 0.013° from 1.004° to 28° 2 $\theta$ , and the measuring time was 2.5 min per pattern.

Micro-Raman spectra were measured with a dispersive Jobin-Yvon Lab Ram HR 800 spectrometer, with a 532 nm line as the excitation source. The laser power was 6 mW at the sample point. The detector was a CCD, which was cooled at -70 °C. The spectrometer was coupled to an optic microscope Olympus BXFM (50×). A Linkam THMG600/720 stage with a PE95/T95 temperature controller and an LNP liquid-nitrogen cooling system was installed on the microscope. Samples were put on an aluminum sample cell in the Linkam stage. Raman spectra were obtained for an exposure time of 15 s. The coupling of the Linkam stage and the micro-Raman equipment permitted us to follow thermal treatments closely, controlling the cooling and heating rates in a wide temperature range.

## RESULTS AND DISCUSSION

**General Polymorphic Properties.** Table 1 summarizes the melting points and long/short-spacing values of the polymorphs of OOO and OOL examined in the present work.

Long-spacing values were used for determining the chain-length structures, whereas short-spacing values permitted us to identify the polymorphic forms. These polymorphic forms are defined according to their subcell structures, which correspond to cross-sectional packing modes of the zigzag aliphatic chains.<sup>1</sup>

**Table 1. Long and Short Spacing Values of the Polymorphic Forms of OOO and OOL**

	melting temperature (°C)	long spacing, nm	short spacing, nm
			OOO
$\alpha$ -2	-33	4.5	0.431 with shoulder
$\beta'_2$ -2		4.5	0.434, 0.405
$\beta'_1$ -2	-13	4.5	0.452, 0.436, 0.407, 0.393
$\beta_2$ -2	-2	4.4	0.458 (0.456), 0.448, 0.398, 0.389, 0.378
$\beta_1$ -2	2.9	4.4	0.458 (0.456), 0.448, 0.435, 0.405, 0.399, 0.387, 0.381, 0.377, 0.374, 0.368
			OOL
$\alpha$ -2	-60	4.4	0.421 with shoulder
$\beta'_2$ -2	-25	4.4	0.433, 0.410
$\beta'_1$ -2	21	4.5	0.453, 0.438, 0.391

Thus, in general, the  $\alpha$  form is defined by a hexagonal subcell (H), the  $\beta'$  form has an orthorhombic perpendicular subcell ( $O_{\perp}$ ), and the subcell of  $\beta$  form is triclinic parallel ( $T_{//}$ ). The XRD data of the three forms of OOO ( $\alpha$ ,  $\beta'$ , and  $\beta$ ) have been determined in previous studies<sup>16,19</sup> whose data are in good agreement with those reported in the present study. In addition, we observed the long- and short-spacing values of two  $\beta'$  forms ( $\beta'_{2}$  and  $\beta'_{1}$ ) and two  $\beta$  forms ( $\beta_2$  and  $\beta_1$ ) of OOO. Previously, Hagemann et al.<sup>17</sup> confirmed the existence of three  $\beta'$  forms ( $\beta'_{3}$ ,  $\beta'_{2}$ , and  $\beta'_{1}$ ). Using IR, they could determine the typical orthorhombic subcell structure of  $\beta'$  form and the DSC data permitted to differentiate three  $\beta'$  forms; however, no XRD data were given. Akita et al.<sup>19</sup> reported only one form of  $\beta'$  and  $\beta$ , corresponding to  $\beta'_{1}$  and  $\beta_1$  of the present study, in accordance with the melting points.

No  $\beta$  form was observed for OOL, since the short-spacing pattern of 0.458 nm, which is typical of the triclinic subcell of  $\beta$  form, was not detectable. Instead, two  $\beta'$  forms were observed as the most stable polymorphs.

The chain-length structures of all the polymorphic forms of OOO and OOL are double (Table 1). From the long-spacing values observed, we can conclude that the inclination angles are relatively large, even in the  $\alpha$  phases. Compared with the long-spacing values of the corresponding trisaturated TAG (tristearin (SSS)), the difference in the long-spacing values between polymorphs of OOO and OOL is much smaller. SSS exhibits long spacing at 5.06, 4.72, and 4.50 nm for the corresponding polymorphs ( $\alpha$ ,  $\beta'$ , and  $\beta$ ).<sup>21</sup> The large long-spacing value of  $\alpha$  of SSS is due to the perpendicular orientation of the acyl chains against the lamellar surface, and the acyl chains are more inclined in the order of  $\beta'$  and  $\beta$ . Therefore, the smaller long-spacing value of  $\alpha$  form for OOO and OOL than for SSS may indicate that the presence of cis double bonds may shorten lamellar distance. The structure models of OOO and OOL will be discussed later.

**Polymorphic Characteristics of OOO.** Figure 1 depicts the DSC thermograms of OOO taken by cooling from the melt at different rates (15, 2, 1, and 0.5  $^{\circ}\text{C}\cdot\text{min}^{-1}$ ) and heated at 15  $^{\circ}\text{C}\cdot\text{min}^{-1}$ .

The DSC data, including the onset temperature ( $T_{\text{onset}}$ ) and enthalpy ( $\Delta H$ ) associated with each transition, are presented in Table 2.

To identify the crystallization and transformation processes of the polymorphic forms exhibited in exothermic and endothermic DSC peaks, we conducted SR-XRD experiments by applying the same thermal treatments as DSC (Figure 2).

When the cooling rate was 15  $^{\circ}\text{C}\cdot\text{min}^{-1}$ , we observed the crystallization of  $\alpha$  at  $-51.1\ ^{\circ}\text{C}$ , indicated by the long-spacing peak of 4.5 nm and short-spacing peak of 0.431 nm (Figure 2). However, the more stable  $\beta'_{2}$  form crystallized with the decreased cooling rates of 2, 1, and 0.5  $^{\circ}\text{C}\cdot\text{min}^{-1}$ . The transformation pathways to more stable forms differed when starting from  $\alpha$  or  $\beta'_{2}$  crystals, although the  $\beta$  phase was reached as the most stable form in both cases. The details of the experimental results are explained below.

After crystallization of  $\alpha$  by cooling at 15  $^{\circ}\text{C}\cdot\text{min}^{-1}$ , very complicated transformation processes occurred from  $\alpha$  to  $\beta$  forms through intermediate forms during heating at 15  $^{\circ}\text{C}\cdot\text{min}^{-1}$ , as demonstrated in a series of DSC endothermic and exothermic peaks (Figure 1a) and changes in the SR-XRD WAXD patterns (Figure 2a). First, melt-mediated transition occurred from  $\alpha$  (melting at  $-34.1\ ^{\circ}\text{C}$ ) to  $\beta'_{2}$  (crystallization at  $-32.3\ ^{\circ}\text{C}$ ). Although not detected in DSC peaks, transformation from  $\beta'_{2}$  to  $\beta'_{1}$  was observed at  $-20\ ^{\circ}\text{C}$ , as indicated in the SR-

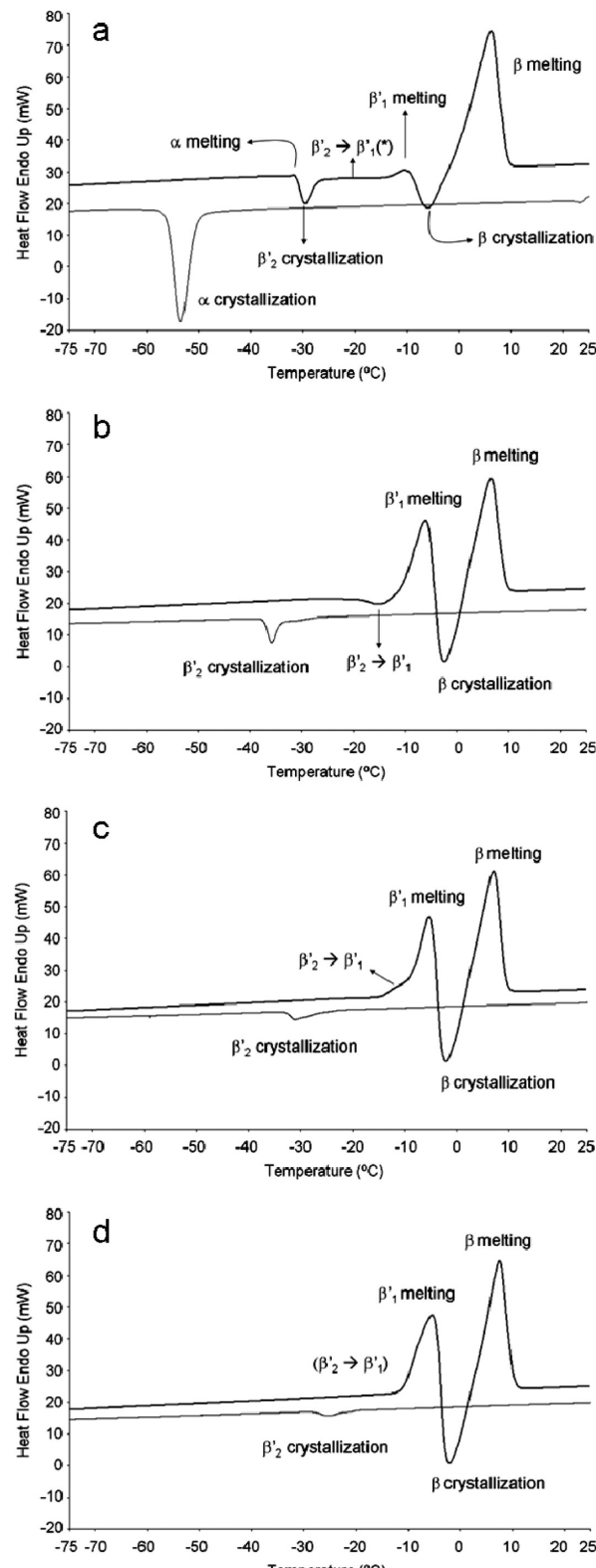


**Figure 1.** DSC thermograms of OOO obtained by applying different cooling rates (heating rate was always 15  $^{\circ}\text{C}\cdot\text{min}^{-1}$ ): (a) 15, (b) 2, (c) 1, and (d) 0.5  $^{\circ}\text{C}\cdot\text{min}^{-1}$ .

XRD patterns (Figure 2a). Another melt-mediated transformation then occurred from  $\beta'_{1}$  (melting at  $-14.4\ ^{\circ}\text{C}$ ) to  $\beta$  (crystallization at  $-10.2\ ^{\circ}\text{C}$ ). Finally,  $\beta$  melted at  $-3.3\ ^{\circ}\text{C}$ .

**Table 2.** DSC Data of the Polymorphic Crystallization and Transformation of OOO Obtained When the Sample Was Cooled and Heated at Different Rates<sup>a</sup>

polymorph	Cooling ( $15\text{ }^{\circ}\text{C}\cdot\text{min}^{-1}$ )			Heating ( $15\text{ }^{\circ}\text{C}\cdot\text{min}^{-1}$ )		
	$\alpha$ (c)	$\alpha$ (m)	$\beta'_2$ (c)	$\beta'_1$ (m)	$\beta$ (c)	$\beta$ (m)
$T\text{ (}^{\circ}\text{C)}$	$-51.1 \pm 0.6$	$-34.1 \pm 0.5$	$-32.3 \pm 0.5$	$-14.4 \pm 0.5$	$-10.2 \pm 0.8$	$-3.3 \pm 0.8$
$\Delta H\text{ (J/g)}$	$-54 \pm 2$	approx 0	$-9 \pm <1$	$2 \pm 1$	$-16 \pm 2$	$105 \pm 17$
polymorph	Cooling ( $2\text{ }^{\circ}\text{C}\cdot\text{min}^{-1}$ )			Heating ( $15\text{ }^{\circ}\text{C}\cdot\text{min}^{-1}$ )		
	$\beta'_2$ (c)	$\beta'_2 \rightarrow \beta'_1$	$\beta'_1$ (m)	$\beta$ (c)	$\beta$ (m)	
$T\text{ (}^{\circ}\text{C)}$	$-26.6 \pm 1.2$	$-33.4 \pm 0.7$	$-20.8 \pm 1.3$	$-13.3 \pm 0.6$	$-5.3 \pm 0.4$	$0.4 \pm 0.4$
$\Delta H\text{ (J/g)}$	$-70 \pm 1$		$-6 \pm 3$	$41 \pm 2$	$-33 \pm 3$	$73 \pm 3$
polymorph	$(2\text{ }^{\circ}\text{C}\cdot\text{min}^{-1})$			$(2\text{ }^{\circ}\text{C}\cdot\text{min}^{-1})$		
	$\beta'_2 \rightarrow \beta'_2$	$\beta_2 \rightarrow \beta_1$	$\beta_2 \rightarrow \beta_1$ (m)			
	$-25 \pm 1.7$	$-11.3 \pm 1.7$	$-2.2 \pm 0.7$	$2.9 \pm 1.3$		
$T\text{ (}^{\circ}\text{C)}$		$b$	$-27 \pm 4$	$128 \pm 5^c$		
polymorph	Cooling ( $1\text{ }^{\circ}\text{C}\cdot\text{min}^{-1}$ )			Heating ( $15\text{ }^{\circ}\text{C}\cdot\text{min}^{-1}$ )		
	$\beta'_2$ (c)	$\beta'_2 \rightarrow \beta'_1$	$\beta'_1$ (m)	$\beta$ (c)	$\beta$ (m)	
	$-22.3 \pm 0.7$	$26.3 \pm 3.1$	$-15.7 \pm 0.8$	$-11.2 \pm 0.4$	$-5.0 \pm 0.6$	$0.6 \pm 0.5$
$\Delta H\text{ (J/g)}$	$-76 \pm 3$		$40 \pm 2^c$	$-31 \pm 2$	$71 \pm 2$	
polymorph	Cooling ( $0.5\text{ }^{\circ}\text{C}\cdot\text{min}^{-1}$ )			Heating ( $15\text{ }^{\circ}\text{C}\cdot\text{min}^{-1}$ )		
	$\beta'_2$ (c)	$\beta'_1$ (m)	$\beta$ (c)	$\beta$ (m)		
	$-19.1 \pm 1.5$	$21.5 \pm 0.7$	$-12.2 \pm 1.2$	$-4.5 \pm 1.1$	$1.3 \pm 1$	
$\Delta H\text{ (J/g)}$	$-83 \pm 5$		$45 \pm 4$	$-33 \pm 6$	$73 \pm 8$	

<sup>a</sup>The letters c, s, and m mean crystallization, solid-state transformation, and melting, respectively. <sup>b</sup>It was not possible to determine this value because the nature of this transformation pathway is not clear (see text). <sup>c</sup>These enthalpy values correspond to the global enthalpy of overlapped peaks.

In the SR-XRD patterns, the  $\beta'_2$  form was identified by two new WAXD peaks with  $d$ -spacing values of 0.434 and 0.405 nm for  $\beta'_2$ , although the SAXD peak was maintained. On further heating, a new peak at 0.393 nm for  $\beta'_1$  was detected in the WAXD pattern, corresponding to transformation from  $\beta'_2$  to  $\beta'_1$ ; however, no transition was observed in the DSC thermogram in the same temperature range.  $\beta'_1$  melted at  $-14.4\text{ }^{\circ}\text{C}$  ( $T_{\text{onset}}$ ); soon after, the  $\beta$  form crystallized at  $-10.2\text{ }^{\circ}\text{C}$  (melt-mediated transition). This was confirmed by a shift from 4.5 to 4.4 nm in the SAXD pattern and by the most representative WAXD peaks with  $d$ -spacing values of 0.456, 0.448, 0.398, 0.389, and 0.376 nm. This form finally melted at  $-3.3\text{ }^{\circ}\text{C}$  ( $T_{\text{onset}}$ ).

When the cooling rate was decreased to 2, 1, or  $0.5\text{ }^{\circ}\text{C}\cdot\text{min}^{-1}$ , the  $\beta'_2$  form (instead of  $\alpha$ ) was obtained from the melt, as indicated by the SAXD peak at 4.5 nm and two WAXD peaks with  $d$ -spacing values of 0.434 and 0.405 nm (Figure 2b–d). The crystallization temperatures of  $\beta'_2$  increased with decreasing cooling rates as follows:  $-26.6\text{ }^{\circ}\text{C}$  at  $2\text{ }^{\circ}\text{C}\cdot\text{min}^{-1}$ ,  $-22.3\text{ }^{\circ}\text{C}$  at  $1\text{ }^{\circ}\text{C}\cdot\text{min}^{-1}$ , and  $-19.1\text{ }^{\circ}\text{C}$  at  $0.5\text{ }^{\circ}\text{C}\cdot\text{min}^{-1}$ . In these three cases, two onset temperatures were determined for the  $\beta'_2$  crystallization peak (Table 2), as the complex DSC signal consisted of a main exothermic peak having a shoulder. Nevertheless, the beginning of the crystallization phenomenon corresponded to the first determined onset temperature. The transformation pathways from the starting polymorph  $\beta'_2$  on heating were  $\beta'_2 \rightarrow \beta'_1 \rightarrow$  liquid  $\rightarrow \beta \rightarrow$  liquid when the heating rate was  $15\text{ }^{\circ}\text{C}\cdot\text{min}^{-1}$ . Transformation into  $\beta'_1$  was indicated by XRD peaks at 0.452, 0.436, 0.407, and 0.393 nm (WAXD pattern).

Even though the SR-XRD patterns exhibiting  $\beta'_2 \rightarrow \beta'_1$  transformation on heating were quite similar to the three different cooling rates, the DSC patterns differed. When the cooling rate was  $2\text{ }^{\circ}\text{C}\cdot\text{min}^{-1}$ , the  $\beta'_2 \rightarrow \beta'_1$  transformation appeared as an exothermic DSC peak with an onset temperature of  $-20.8\text{ }^{\circ}\text{C}$ . However, when the cooling rate was  $1\text{ }^{\circ}\text{C}\cdot\text{min}^{-1}$ , this peak became endothermic ( $T_{\text{onset}} = -15.7\text{ }^{\circ}\text{C}$ ), and no peak

was observed when the cooling rate was  $0.5\text{ }^{\circ}\text{C}\cdot\text{min}^{-1}$ . Because no significant differences were detected in the SR-XRD patterns corresponding to the  $\beta'_2 \rightarrow \beta'_1$  transformation in the three cases described above, no definitive explanation can be extracted from the different thermal behaviors observed. The variation of the cooling rate from 2 to  $0.5\text{ }^{\circ}\text{C}\cdot\text{min}^{-1}$  may have influenced the subsequent  $\beta'_2 \rightarrow \beta'_1$  transition, which occurred on the heating process. Probably, by varying the cooling rate, the crystallization process occurred through different mechanisms (e.g., the transformation from  $\beta'_2$  to  $\beta'_1$  may have partially occurred during cooling at 1 and  $0.5\text{ }^{\circ}\text{C}\cdot\text{min}^{-1}$ , although not revealed by the SR-XRD data).

After the  $\beta'_2 \rightarrow \beta'_1$  transition, the melt-mediated transformation from  $\beta'_1$  to  $\beta$  occurred on heating at a rate of  $15\text{ }^{\circ}\text{C}\cdot\text{min}^{-1}$ . The DSC patterns clearly exhibited endothermic peaks of  $\beta'_1$  melting at  $-11$  to  $-13\text{ }^{\circ}\text{C}$ , which is associated with exothermic peaks of  $\beta$  crystallization at  $-6$  to  $-4\text{ }^{\circ}\text{C}$  (Figure 1). Furthermore,  $\beta$  was easily identified by the shifting of the SAXD peak from 4.5 to 4.4 nm and the 0.458, 0.448, 0.398, 0.389, and 0.376 nm WAXD peaks (Figure 2). Finally, the  $\beta$  form melted at 0.4 to 1.3  $^{\circ}\text{C}$ . The temperatures of melting of  $\beta'_1$ , crystallization, and melting of  $\beta$  somehow varied when the applied cooling rates changed from 2, 1, and  $0.5\text{ }^{\circ}\text{C}\cdot\text{min}^{-1}$ . However, taking into account the error associated with the values given by the DSC data (see Table 2), we can assume that the temperatures at which each phenomenon occurred when different cooling rates were used are comparable.

It is noteworthy that the transformation characteristics from  $\beta'_2$ , which occurred after crystallization at the cooling rate of  $2\text{ }^{\circ}\text{C}\cdot\text{min}^{-1}$ , changed when the heating rate was decreased from  $15\text{ }^{\circ}\text{C}\cdot\text{min}^{-1}$  to  $2\text{ }^{\circ}\text{C}\cdot\text{min}^{-1}$  (Figure 3).

Here, two  $\beta$  forms ( $\beta_2$  and  $\beta_1$ ) could be distinguished, as confirmed by the SR-XRD data and by the presence of a narrow melting peak with a shoulder at high temperatures in the DSC profile. Two consecutive transitions took place, from  $\beta'_2$  to  $\beta_2$  at a

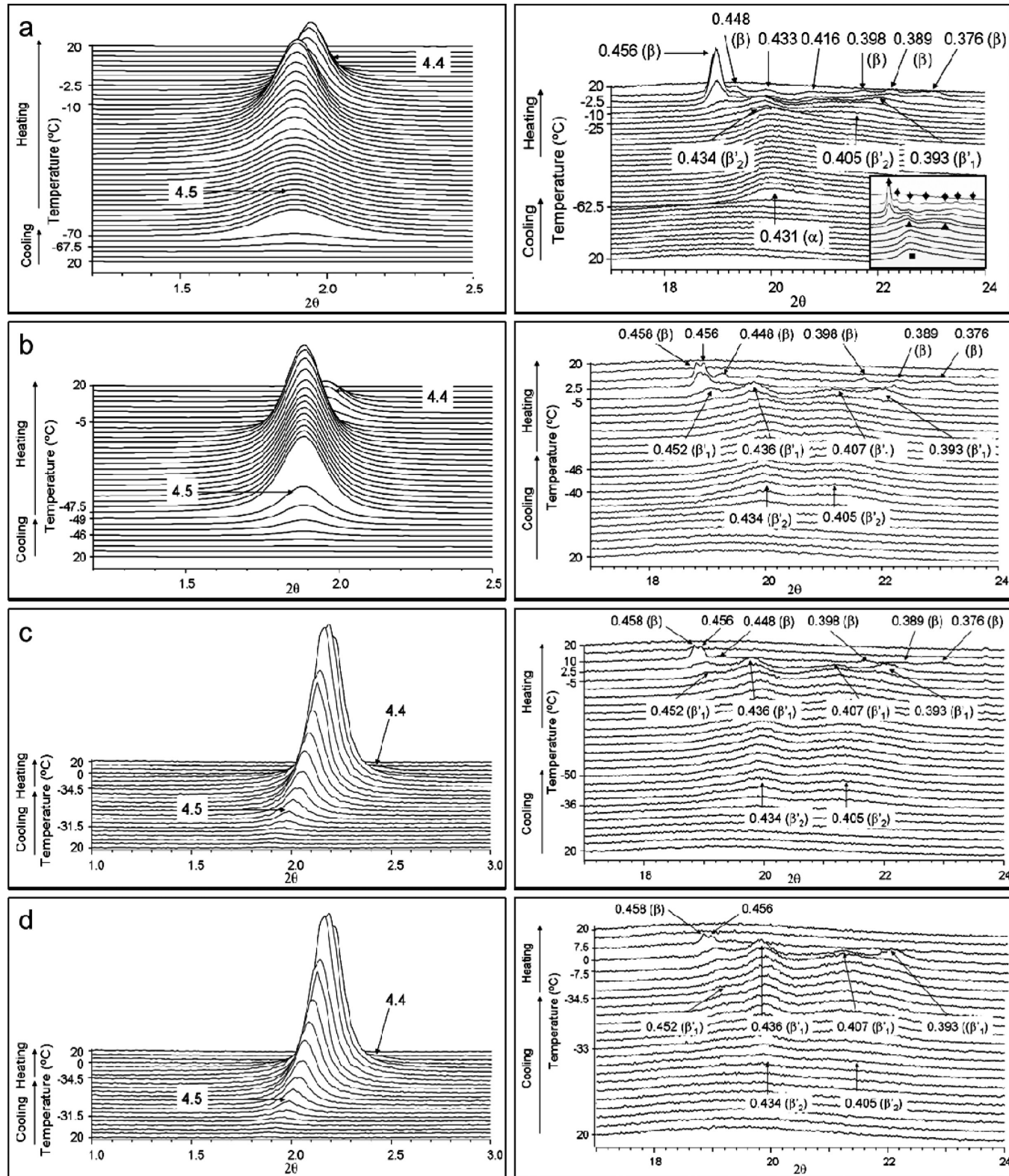


**Figure 2.** SR-XRD patterns of OOO obtained by applying different cooling rates (heating rate was always  $15\text{ }^{\circ}\text{C}\cdot\text{min}^{-1}$ ): (a) 15, (b) 2, (c) 1, and (d)  $0.5\text{ }^{\circ}\text{C}\cdot\text{min}^{-1}$ . SAXD pattern (left) and SR-WAXD pattern (right). Inserted figure in panel a shows, in more detail,  $\alpha$  (squares),  $\beta'$  (triangles), and  $\beta$  (diamonds) SR-WAXD peaks.

$T_{\text{onset}}$  of  $-25\text{ }^{\circ}\text{C}$  and from  $\beta_2$  to  $\beta_1$  at a  $T_{\text{onset}}$  of  $-11.3\text{ }^{\circ}\text{C}$  (insert in Figure 3a). It was difficult to clearly define the nature of the transformation pathway from  $\beta'_2$  to  $\beta_2$ ; however, the shape of the DSC peak indicated that the transition might occur through melt-mediated transformation with a broad and flat melting peak.

At  $-33\text{ }^{\circ}\text{C}$ , some changes could be observed in the SR-XRD WAXD pattern (e.g., decreased peak intensity), possibly due to some melting. Nevertheless, the only phenomenon that was easy to identify in the DSC profile was the exothermic peak with an onset temperature of  $-25\text{ }^{\circ}\text{C}$ . We could easily detect the  $\beta_2$  form

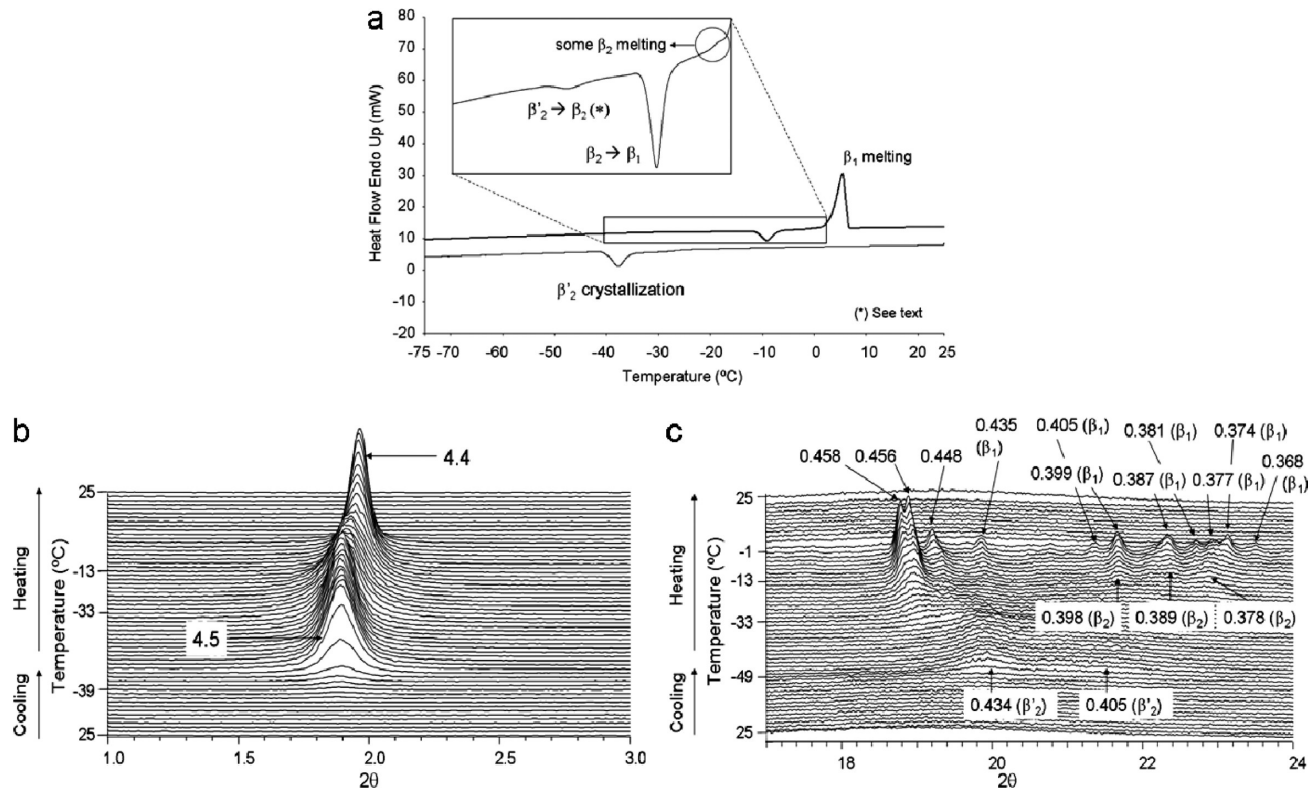


**Figure 3.** Polymorphic behavior of OOO when cooled at  $2\text{ }^{\circ}\text{C}\cdot\text{min}^{-1}$  ( $\beta'_3$  crystallization) and heated at  $2\text{ }^{\circ}\text{C}\cdot\text{min}^{-1}$ : (a) DSC thermogram, (b) SR-SAXD pattern, and (c) SR-WAXD pattern.

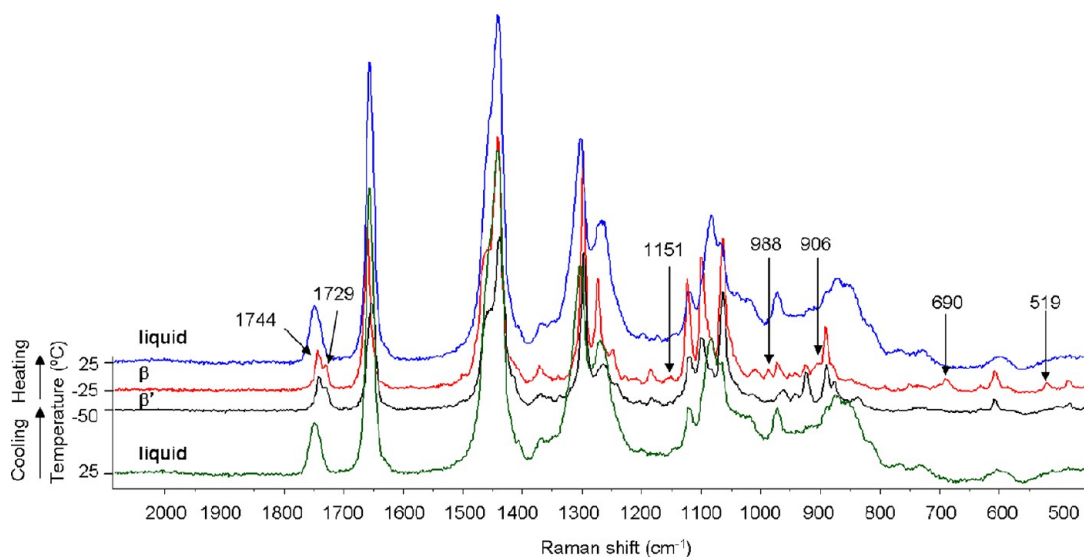


**Figure 4.** Raman spectra of OOO taken during cooling and heating processes at  $2\text{ }^{\circ}\text{C}\cdot\text{min}^{-1}$ .

through the WAXD peaks at 0.458, 0.398, 0.389, and 0.378 nm. On further heating, another transformation (with  $T_{\text{onset}} = -11.3\text{ }^{\circ}\text{C}$ ) occurred to obtain another  $\beta$  form ( $\beta_1$ ). Hence, we could distinguish between two  $\beta$  forms in OOO because the typical WAXD peaks of  $\beta$  were maintained, but a clear change was observed when new WAXD peaks of  $\beta_1$  appeared at 0.381, 0.374, and 0.368 nm. The melting curve of these two  $\beta$  forms appeared as a sharp melting peak (narrower than in the cases described above) with a  $T_{\text{onset}}$  of  $2.9\text{ }^{\circ}\text{C}$  (due to  $\beta_1$  melting), revealing a clear shoulder at  $-2.2\text{ }^{\circ}\text{C}$  ( $\beta_2$  melting). Therefore, because some  $\beta_2$  melting was observed, we can conclude that not all  $\beta_2$

transformed to  $\beta_1$  because some melted at a higher temperature than that of the  $\beta_2 \rightarrow \beta_1$  transformation. Comparison of the  $\Delta H$  values associated with  $\beta$  melting when OOO was cooled at  $2\text{ }^{\circ}\text{C}\cdot\text{min}^{-1}$  and heated at  $15\text{ }^{\circ}\text{C}\cdot\text{min}^{-1}$  (melting  $\Delta H$  of  $73\text{J}\cdot\text{g}^{-1}$ ) and  $2\text{ }^{\circ}\text{C}\cdot\text{min}^{-1}$  (melting  $\Delta H$  of  $128\text{J}\cdot\text{g}^{-1}$ ) indicates an increase in the amount of  $\beta$  obtained as the heating rate was decreased. Two  $\beta$  forms of OOO were previously indicated,<sup>18</sup> and the present study clearly confirmed it using SR-XRD data.

Micro-Raman experiments were carried out to study the polymorphic transformations that occurred when OOO was cooled and heated at  $2\text{ }^{\circ}\text{C}\cdot\text{min}^{-1}$  (Figure 4). Clear differences

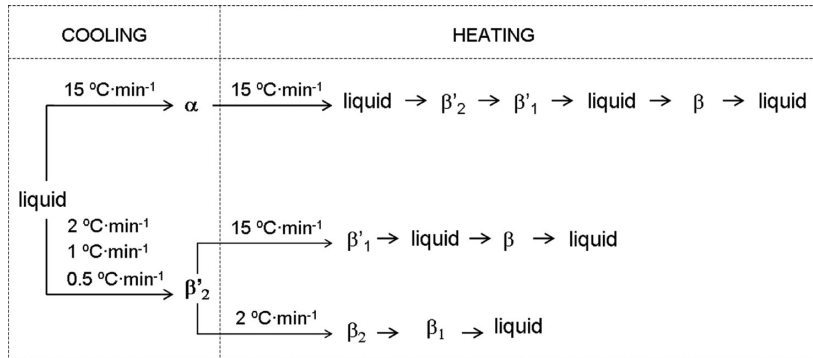


Figure 5. Polymorphic crystallization and transformation pathways of OOO under different cooling and heating conditions.

Table 3. DSC data of the polymorphic crystallization and transformation of OOLi obtained when the sample was cooled and heated at different rates<sup>a</sup>

polymorph	Cooling (15 °C·min <sup>-1</sup> )		Heating (15 °C·min <sup>-1</sup> )	
	α (c)	α (m)	β'₂ (c)	β'₂ + β'₁ (m)
T <sub>onset</sub> (°C)	b	-65.5 ± 1.1	-57.8 ± 0.2	-25.4 ± 0.5
ΔH (J/g)		2 ± 1	-11 ± 2	72 ± 4 <sup>c</sup>
		(0.5 °C·min <sup>-1</sup> )		
polymorph	α → β'₂		β'₁ (m)	
T <sub>onset</sub> (°C)		-65.2 ± 0.3	-20.9 ± 0.4	
ΔH (J/g)		-5 ± 2	79 ± 3	
polymorph	Cooling (2 °C·min <sup>-1</sup> )		Heating (2 °C·min <sup>-1</sup> )	
	β'₁ (c)	β'₁ (m)		
T <sub>onset</sub> (°C)	-41.6 ± 0.4	-20.4 ± 0.8		
ΔH (J/g)	-61 ± 4	73 ± 3		
polymorph	Cooling (0.5 °C·min <sup>-1</sup> )		Heating (15 °C·min <sup>-1</sup> )	
	β'₁ (c)	β'₁ (m)		
T <sub>onset</sub> (°C)	-33.4 ± 0.6	-21.9 ± 0.5		
ΔH (J/g)	-72 ± 4	80 ± 4		

<sup>a</sup>The letters c, s, and m mean crystallization, solid-state transformation, and melting, respectively. DSC onset temperatures were defined for crystallization and melting. <sup>b</sup>The α crystallization occurred during the isothermal and the beginning of the heating processes, so the DSC peak could not be interpreted as a function of temperature. <sup>c</sup>These enthalpy values correspond to the global enthalpy of overlapped peaks.

were observed in the spectra corresponding to the liquid state, β' and β forms. However, it was not possible to identify the two β forms.

At -50 °C, the β' form was detected; at -25 °C, it transformed to the β form on heating. As Akita et al.<sup>19</sup> reported, the carbonyl stretch [ $\nu(C=O)$ ] band at 1749 cm<sup>-1</sup> in the liquid state split into two bands at 1744 and 1729 cm<sup>-1</sup> in the β form. Subtle splitting could also be observed in the Raman spectrum corresponding to the β' form. According to Akita et al.,<sup>19</sup> the Raman C=C stretching band  $\nu(C=C)$  is a good indicator of the conformation of the *cis*-olefin group. Thus, the band at 1653 cm<sup>-1</sup> in the β' form shifted to 1660 cm<sup>-1</sup> in the β form. Moreover, additional bands appeared at 1151, 988, 906, 690, and 519 cm<sup>-1</sup> when the β' transformed to the β form.

Figure 5 summarizes the polymorphic crystallization and transformation pathways of OOO.

The α form was obtained by cooling OOO at 15 °C·min<sup>-1</sup>. This α form did not exhibit the typical sharp WAXD peak of 0.41 nm, corresponding to the hexagonal (H) subcell structure that appears in saturated, mono-, and diunsaturated TAGs.<sup>7,8</sup> Here, the α form exhibited a broad peak at 0.431 nm with a shoulder peak. This phenomenon has already been reported.<sup>16,19</sup> For this result, Akita et al.<sup>19</sup> indicated an anisotropic lateral packing of hydrocarbon chains and a distorted H subcell structure. It was

evident that the first-occurring polymorph changed from α to β'₂ with decreasing rates of cooling from 15 to 2, 1, and 0.5 °C·min<sup>-1</sup>. We have already observed the same results in OPO<sup>7</sup> and POP.<sup>8</sup>

Regarding the transformation pathways on heating, the polymorphic pathways depended mainly on the heating rate and, as the Ostwald step rule predicts,<sup>22</sup> the first-occurring metastable forms were successively followed by other forms of increasing stability. Thus, the most stable β form was always reached at the two heating rates used (15 and 2 °C·min<sup>-1</sup>) through β'₂ and β'₁. Furthermore, when OOO was heated at the lower heating rate (2 °C·min<sup>-1</sup>), it was possible to distinguish the two β forms (β₂ and β₁).

**Polymorphic Characteristics of OOL.** OOL was also subjected to different thermal programs. Table 3 summarizes the melting temperatures and ΔH values when different rates of cooling (15, 2, and 0.5 °C·min<sup>-1</sup>) and heating (15, 2, and 0.5 °C·min<sup>-1</sup>) were applied to the OOL samples. No β forms were present, and the most stable polymorph was β'. This result was the same as for 1,2-dipalmitoyl-3-myristoyl-sn-glycerol (PPM),<sup>23</sup> 1,2-dipalmitoyl-3-oleoyl-rac-glycerol (PPO),<sup>24</sup> 1,2-distearoyl-3-oleoyl-rac-glycerol (SSO),<sup>25</sup> 1-palmitoyl-2, 3-oleoyl-rac-glycerol (POO),<sup>26</sup> and 1-stearoyl-2,3-oleoyl-rac-glycerol (SOO),<sup>27</sup> probably because all these TAGs are asymmetric mixed-acid TAGs.

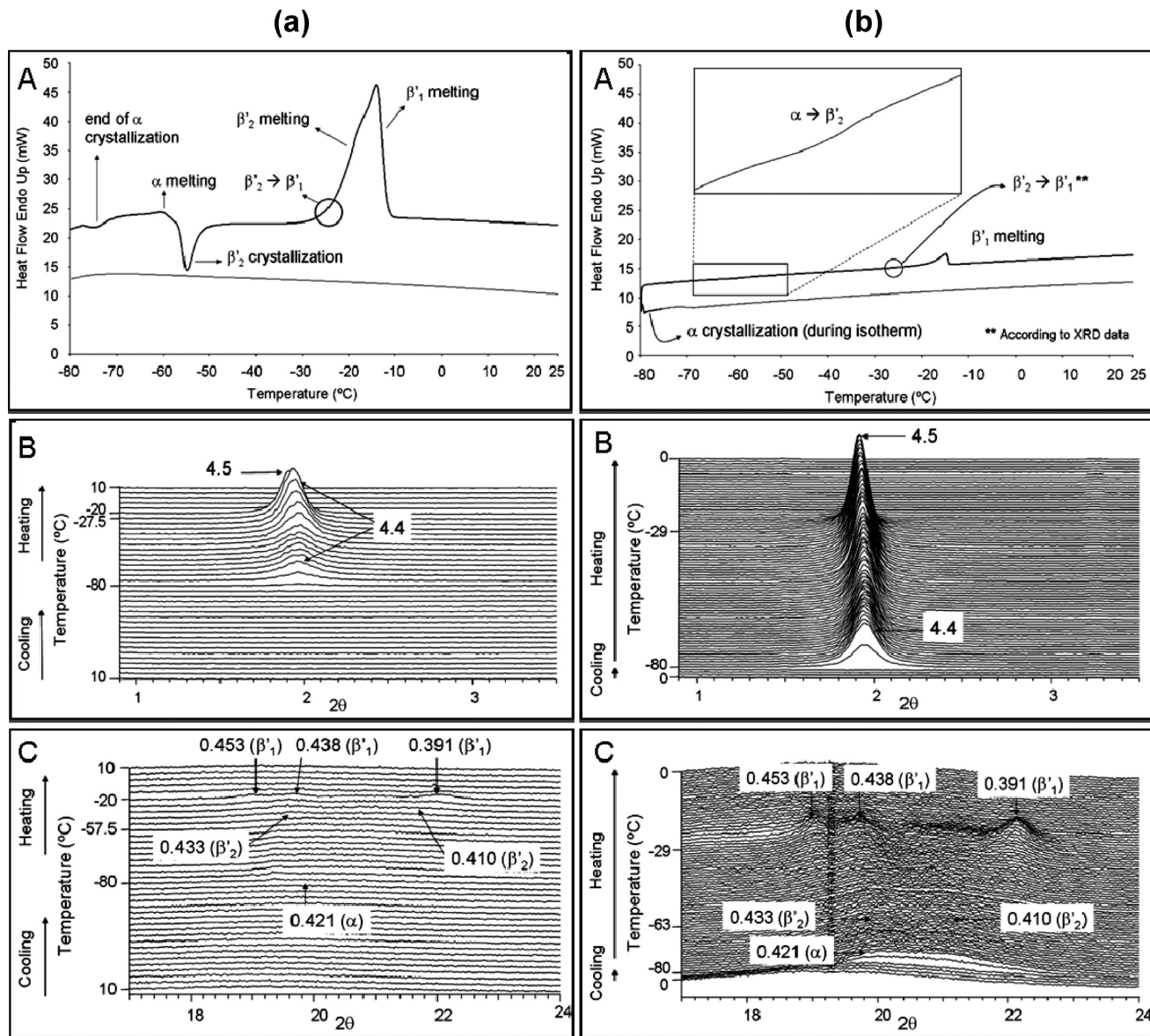


**Figure 6.** Polymorphic behavior of OOL. (a) Cooling at  $15\text{ }^{\circ}\text{C}\cdot\text{min}^{-1}$  and heating at  $15\text{ }^{\circ}\text{C}\cdot\text{min}^{-1}$ : (A) DSC thermogram, (B) SR-SAXD pattern, (C) SR-WAXD pattern. (b) Cooling at  $15\text{ }^{\circ}\text{C}\cdot\text{min}^{-1}$  and heating at  $0.5\text{ }^{\circ}\text{C}\cdot\text{min}^{-1}$ : (A) DSC thermogram, (B) SR-SAXD pattern, (C) SR-WAXD pattern.

The least stable polymorph ( $\alpha$ ) was obtained when the cooling rate was high, whereas the most stable form ( $\beta'$ ) crystallized from the melt at cooling rates of 2 and  $0.5\text{ }^{\circ}\text{C}\cdot\text{min}^{-1}$ . When the heating rate was varied, the most stable  $\beta'$  form was obtained in all cases examined, similar to OOO.

Figure 6 depicts the polymorphic characteristics of OOL when it was cooled at a high rate ( $15\text{ }^{\circ}\text{C}\cdot\text{min}^{-1}$ ) and heated at high ( $15\text{ }^{\circ}\text{C}\cdot\text{min}^{-1}$ ) and low ( $0.5\text{ }^{\circ}\text{C}\cdot\text{min}^{-1}$ ) rates.

At  $15\text{ }^{\circ}\text{C}\cdot\text{min}^{-1}$ , the  $\alpha$  form, with a long spacing of 4.4 nm and a single short spacing of 0.421 nm, crystallized. Similar to OOO, the broad WAXD peak at 0.421 nm had a shoulder. No exothermic DSC peak corresponding to this crystallization was observed in the cooling thermal step because of the low crystallization temperature of this polymorphic form and the high cooling rate used. The  $\alpha$  crystallization started during the isotherm (1 min long) that took place between the cooling and heating steps and ended at the beginning of the heating process (Figure 6(a)A).

After  $\alpha$  crystallization, melt-mediated transformation from  $\alpha$  to  $\beta'_2$  occurred when the sample was heated at  $15\text{ }^{\circ}\text{C}\cdot\text{min}^{-1}$ , as observed in the melting of  $\alpha$  at  $-65.5\text{ }^{\circ}\text{C}$  and the crystallization of  $\beta'_2$  at  $-57.8\text{ }^{\circ}\text{C}$  (Figure 6aA). This was clearly demonstrated by the presence of the  $\beta'_2$  WAXD broad peaks at 0.433 nm and 0.410 nm (Figure 6aB). Later, the SR-XRD data indicated that  $\beta'_2$  transformed to  $\beta'$  before  $\beta'$  melted. During this transformation, the SAXD peak shifted from 4.4 nm to 4.5 nm, and new WAXD peaks of  $\beta'$  appeared at 0.453, 0.438, and 0.391 nm. Apparently, not all  $\beta'_2$  transformed to  $\beta'$  because the last melting peak seemed to be double, with clear onset temperatures of  $-25.4\text{ }^{\circ}\text{C}$  (corresponding to  $\beta'_2$  melting) and  $-24\text{ }^{\circ}\text{C}$  (corresponding to  $\beta'$  melting).

Solid-state  $\alpha \rightarrow \beta'_2$  transformation occurred at a heating rate of  $0.5\text{ }^{\circ}\text{C}\cdot\text{min}^{-1}$ , as indicated by an exothermic DSC peak (insert in Figure 6bA). This contrasts with the melt-mediated  $\alpha \rightarrow \beta'_2$  transformation obtained by heating at  $15\text{ }^{\circ}\text{C}\cdot\text{min}^{-1}$ . This solid-state transformation occurred at  $-65.2\text{ }^{\circ}\text{C}$ ; concurrently,  $\beta'_2$  WAXD peaks of 0.433 and 0.410 nm appeared. Later,  $\beta'_2 \rightarrow \beta'$

transformation occurred at  $-39^{\circ}\text{C}$ , as indicated by the SAXD peak shifting from 4.4 to 4.5 nm and WAXD peaks at 0.453, 0.438, and 0.391 nm, although no DSC thermopeaks were observed. The  $\beta'_1$  form finally melted at  $-20.9^{\circ}\text{C}$ . As explained above, not all  $\beta'_2$  transformed to  $\beta'_1$  at the heating rate of  $15^{\circ}\text{C}\cdot\text{min}^{-1}$  because melting of  $\beta'_2$  was observed together with the melting of  $\beta'_1$ . Not surprisingly,  $\beta'_2$  had enough time to transform completely to  $\beta'_1$ , and  $\beta'_1$  melted afterward at a lower heating rate of  $0.5^{\circ}\text{C}\cdot\text{min}^{-1}$ .

The effects of the decreased cooling rate on the polymorphic crystallization of OOL were clearly observed. Figure 7 depicts the DSC and laboratory-scale XRD data of OOL when it was cooled and heated at  $2^{\circ}\text{C}\cdot\text{min}^{-1}$ .

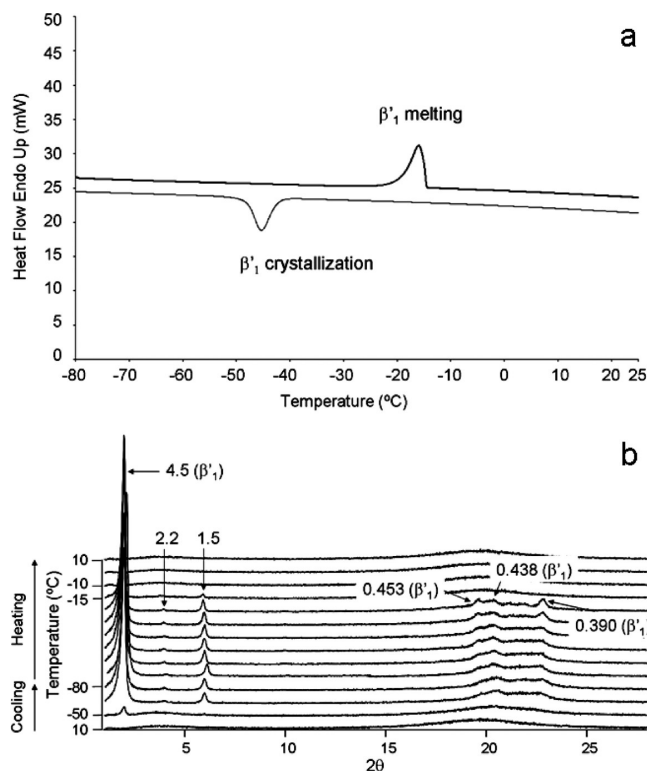


**Figure 7.** Polymorphic behavior of OOL when cooled at  $2^{\circ}\text{C}\cdot\text{min}^{-1}$  ( $\beta'_1$  crystallization) and heated at  $2^{\circ}\text{C}\cdot\text{min}^{-1}$ : (a) DSC thermogram and (b) laboratory-scale XRD pattern.

Figure 8 presents the results obtained for cooling at  $0.5^{\circ}\text{C}\cdot\text{min}^{-1}$  and heating at  $15^{\circ}\text{C}\cdot\text{min}^{-1}$ .

When lower cooling rates were applied (2 and  $0.5^{\circ}\text{C}\cdot\text{min}^{-1}$ ), the first-occurring form was the most stable  $\beta'_1$ . The crystallization temperatures of  $\beta'_1$  were  $-41.6^{\circ}\text{C}$  for cooling at  $2^{\circ}\text{C}\cdot\text{min}^{-1}$  and  $-33.4^{\circ}\text{C}$  for cooling at  $0.5^{\circ}\text{C}\cdot\text{min}^{-1}$ . In both cases, the typical XRD peaks of  $\beta'_1$  were observed, and no  $\beta'_2$  form was present. When  $\beta'_1$  crystals were heated, they simply melted at  $-21$  to  $-20^{\circ}\text{C}$  without transformation to the  $\beta$  form.

Figure 9 summarizes the polymorphic characteristics of OOL observed by varying the cooling and heating rates.

High cooling rates caused the crystallization of  $\alpha$  (least stable form), whereas intermediate and low cooling rates led to the crystallization of the most stable  $\beta'_1$  form. Starting from  $\alpha$  crystals, the sequence of polymorphs of increasing stability when the heating rate was high ( $15^{\circ}\text{C}\cdot\text{min}^{-1}$ ) was  $\alpha \rightarrow$  liquid  $\rightarrow \beta'_2 \rightarrow \beta'_1 \rightarrow$  liquid; however, when the heating rate was low ( $0.5^{\circ}\text{C}\cdot\text{min}^{-1}$ ), it changed to  $\alpha \rightarrow \beta'_2 \rightarrow \beta'_1 \rightarrow$  liquid. The difference

between the two pathways was apparent in the nature of the  $\alpha \rightarrow \beta'_2$  transition: melt-mediated at  $15^{\circ}\text{C}\cdot\text{min}^{-1}$  and solid-state at  $0.5^{\circ}\text{C}\cdot\text{min}^{-1}$ . This was quite similar to that observed for 1,3-dipalmitoyl-2-oleoyl glycerol (POP).<sup>8</sup>

The present study has demonstrated the following kinetic properties of polymorphic crystallization and transformation of OOO and OOL, which were affected by different thermal treatments.

- (1) Five polymorphs ( $\alpha$ ,  $\beta'_2$ ,  $\beta'_1$ ,  $\beta_2$ , and  $\beta_1$ ) were isolated in OOO; three polymorphs ( $\alpha$ ,  $\beta'_2$ , and  $\beta'_1$ ), in OOL.
- (2) The effects of varying cooling and heating rates were remarkable. More stable polymorphs were crystallized by decreasing the cooling rates, whereas less stable polymorphs were manifested at higher cooling rates.
- (3) Solid-state transformations occurred more easily than melt-mediated transformation when the heating rate was decreased.

These properties were consistent with those observed for POP and OPO, whose crystallization and transformation properties were examined with DSC and SR-XRD at cooling and heating rates of  $15$ – $0.5^{\circ}\text{C}\cdot\text{min}^{-1}$  (Table 4).

For OPO, multiple polymorphic forms involving the most stable  $\beta$  form were obtained, demonstrating complex concurrent crystallization in most cases. For POP, however, it was difficult to obtain stable forms, such as  $\beta'$  and  $\beta$ , even when the cooling rate was lowered to  $0.5^{\circ}\text{C}\cdot\text{min}^{-1}$ ; for example,  $\gamma$  was obtained instead of the  $\beta'$  form. In the present study, for OOO and OOL,  $\alpha$  was crystallized with rapid cooling, and  $\beta'$  was crystallized with slow cooling.

More stable forms (e.g.,  $\beta'$  and  $\beta$ ) were obtained through either solid-state or melt-mediated transformation for OPO, OOO, and OOL, even at a high rate ( $15^{\circ}\text{C}\cdot\text{min}^{-1}$ ). However, it was necessary to decrease the heating rates to  $2$ – $0.1^{\circ}\text{C}\cdot\text{min}^{-1}$  to obtain the most stable  $\beta$  form for POP. Thus, we may conclude that similar characteristics of polymorphic crystallization and transformation were observed for OPO, OOO, and OOL; however, POP differed in the difficulty of obtaining the most stable  $\beta$  form.

We may explain these results by taking into account the activation energies of solid-state and melt-mediated transformations from one polymorphic form to another, as fully discussed for POP.<sup>8</sup> Figure 10 illustrates two typical transformations that take place from a less stable form (A) to a more stable form (B). The rates of transformation are basically determined by the magnitude of the activation free energies ( $\Delta G^\#$ ) involved in each process: the larger the  $\Delta G^\#$ , the lower the transformation rate.

As for solid-state transformation,  $\Delta G_{ss}^\#$  may include excess energy to enable structural changes (e.g., subcell structure and chain-length structure) needed to cause transformation from form A to form B. The rate of the melt-mediated transformation is determined by the magnitude of  $\Delta G_m^\#$  corresponding to the melting of form A and the subsequent crystallization ( $\Delta G_c^\#$ ) of form B. However, the actual rate may be determined by  $\Delta G_c^\#$  because of the ease of melting and the small values of  $\Delta G_m^\#$ .

We may simply assume that the values of  $\Delta G_{ss}^\#$  for transformations involving change from loosely packed subcell structures (e.g., hexagonal ( $\alpha$  polymorph)) to more closely packed subcell structures of  $O_\perp$  ( $\beta'$ ) and  $T_{//}$  ( $\beta$ ) are larger than those from  $O_\perp$  ( $\beta'$ ) to  $T_{//}$  ( $\beta$ ). In addition, the values of  $\Delta G_{ss}^\#$  may be lower for transformation between polymorphs having the

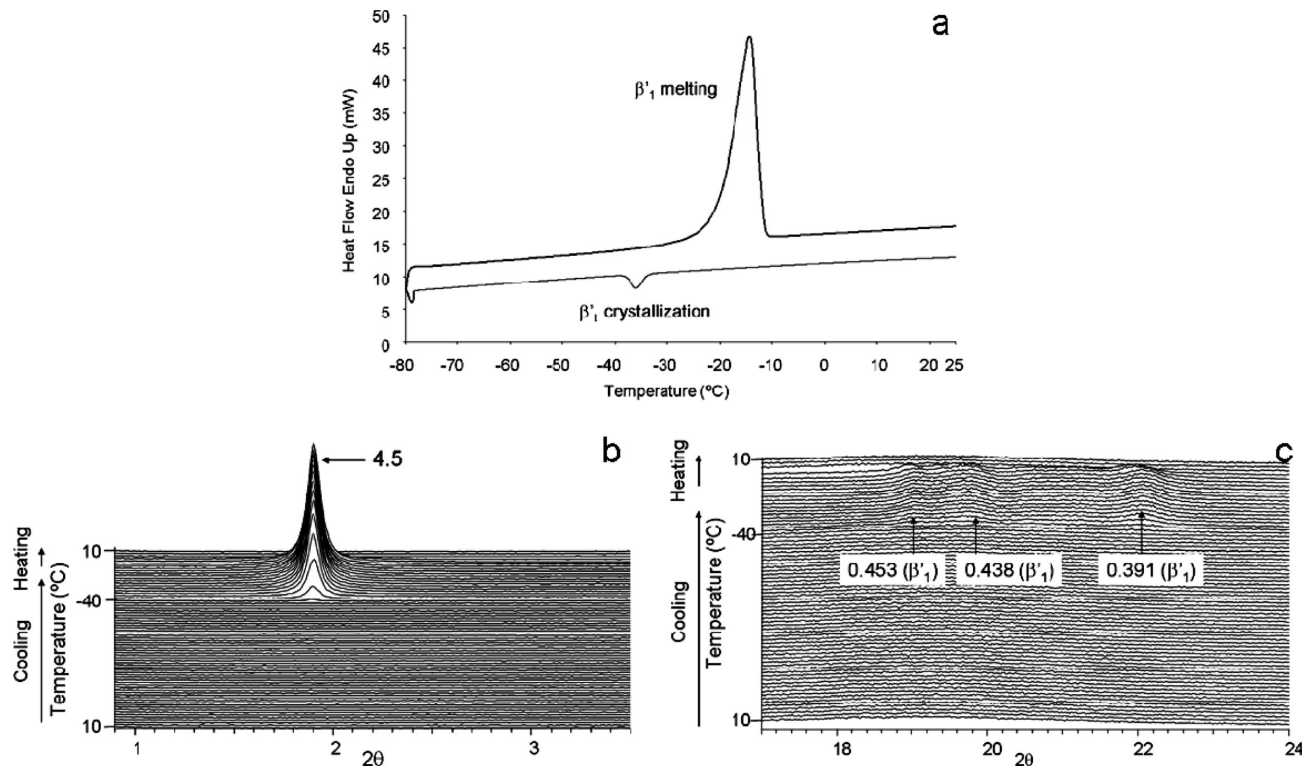


**Figure 8.** Polymorphic behavior of OOL when cooled at  $0.5\text{ }^{\circ}\text{C}\cdot\text{min}^{-1}$  ( $\beta'_1$  crystallization) and heated at  $15\text{ }^{\circ}\text{C}\cdot\text{min}^{-1}$ : (a) DSC thermogram, (b) SR-SAXD pattern, and (c) SR-WAXD pattern.

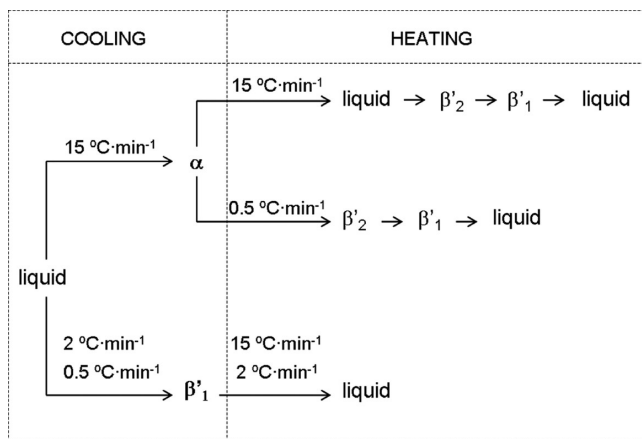


**Figure 9.** Polymorphic crystallization and transformation pathways of OOL under different cooling and heating conditions.

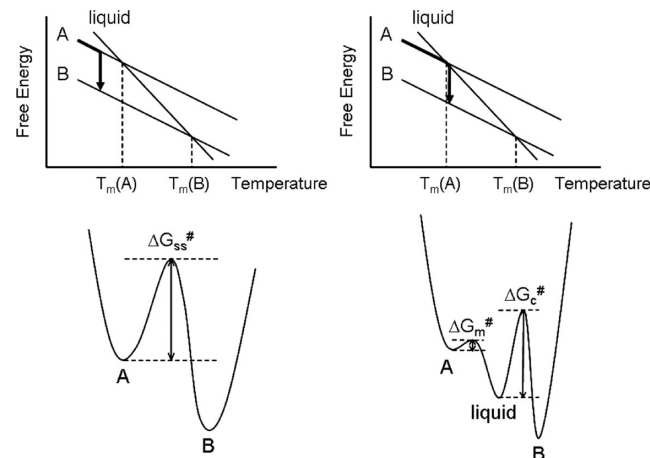


**Figure 10.** Activation free energy ( $\Delta G^\#$ ) for solid-state and melt-mediated transformation from metastable A to more stable B forms.

**Table 4. Crystallization and Transformation Pathways of POP, OPO, OOO and OOL at Different Cooling and Heating Rates, in Which mm and ss Mean Melt-Mediated and Solid-State Transformations**

		POP	OPO	OOO	OOL
polymorphs		$\alpha\text{-}2, \gamma\text{-}3, \beta'\text{-}2^a, \delta\text{-}3, \beta\text{-}3^a$	$\alpha\text{-}2, \beta'\text{-}2^a, \beta\text{-}3$	$\alpha\text{-}2, \beta'\text{-}2^a, \beta\text{-}2^a$	$\alpha\text{-}2, \beta'\text{-}2^a$
crystallization on cooling	rapid	$\alpha$	$\alpha$	$\alpha$	$\alpha$
	slow	$\gamma$	$\beta' + \beta$	$\beta'$	$\beta'$
transformation on heating	rapid	$\alpha \rightarrow (\text{mm})\beta' \rightarrow L$ $\gamma \rightarrow L$	$\alpha \rightarrow (\text{mm})\beta' \rightarrow \beta \rightarrow L$ $\beta' \rightarrow \beta \rightarrow L$	$\alpha \rightarrow (\text{mm})\beta' \rightarrow (\text{mm})\beta \rightarrow L$ $\beta' \rightarrow (\text{mm})\beta \rightarrow L$	$\alpha \rightarrow (\text{mm})\beta' \rightarrow L$ $\beta' \rightarrow L$
	slow	$\alpha \rightarrow \gamma \rightarrow (\text{ss})\delta \rightarrow (\text{mm})\beta \rightarrow L$ $\gamma \rightarrow (\text{mm})\beta' + \delta \rightarrow (\text{mm})\beta \rightarrow L$	na <sup>b</sup>	na <sup>b</sup>	$\alpha \rightarrow (\text{ss})\beta' \rightarrow L$ $\beta' \rightarrow L$

<sup>a</sup>For simplicity,  $\beta'_2$  and  $\beta'_1$  or  $\beta_2$  and  $\beta_1$  are summarized into  $\beta'$  or  $\beta$ , respectively. <sup>b</sup>Not available.

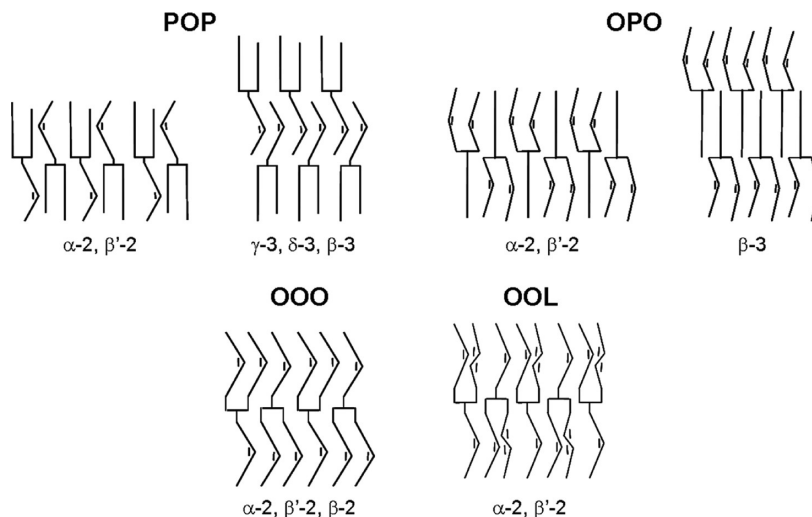


**Figure 11.** Structure models of POP, OPO, OOO, and OOL. For simplicity, multiple  $\beta'$  and  $\beta$  forms are represented by  $\beta'$  and  $\beta$ .

same double chain length structures than for changes from double to triple chain length structures (Figure 11).

The same assumption may apply to crystallization, in that the values of  $\Delta G_c^\#$  of the polymorphs having tightly packed subcell and triple chain length structures may be larger than in the other cases. Taking into account these points, the crystallization and transformation of more stable  $\beta$  and  $\beta'$  forms of OOO and OOL occur easily, since the all polymorphic forms exhibit the same double chain length structure.

A peculiarity in the transformation pathways was observed for POP in that, even during slow heating, solid-state transformation occurred with more difficulty, compared with the OOO and OOL cases. This may be due to the fact that POP contains a saturated fatty acid (palmitic acid) moiety whose transformation from less stable to more stable forms may need large activation energies ( $\Delta G_{ss}^\#$ ) compared with those of oleic and linoleic acid moieties. The flexibility of the chain packing of unsaturated acids is more enhanced than that of saturated fatty acids.<sup>28</sup> This may decrease the value of  $\Delta G_{ss}^\#$  for transformation into more stable forms of OOO and OOL.

To conclude, the present study has found that the occurrence and transformation processes of metastable and more stable polymorphs of OOO and OOL were drastically modified by changing the rates of cooling as well as heating. It may be worth noting that such effects were recently observed in molecular crystals using an ultrafast DSC technique.<sup>29</sup>

## AUTHOR INFORMATION

### Corresponding Author

\*Phone: +34 93 402 13 50. Fax: +34 93 402 13 40. E-mail: laurabayes@ub.edu.

### Notes

The authors declare no competing financial interest.

## ACKNOWLEDGMENTS

The authors acknowledge the financial support of the Ministerio de Economía y Competitividad through Project MAT2011-27225, the Generalitat de Catalunya through the Grup Consolidat (SGR 2009 1307), and the Ministerio de Educación through the Factoría Cristalográfica (Consolider-Ingenio CSD2006-15) and through the Beca del Programa de Formación de Profesorado Universitario (FPU). SR-XRD experiments were

conducted with the approval of the Photon Factory Program Advisory Committee (proposals 2010G114 and 2010G656). The authors gratefully acknowledge the help of Prof. Masaharu Nomura, Station Manager of BL-9C, and Associate Prof. Noriyuki Igarashi, Station Manager of BL-15A at Photon Factory.

## REFERENCES

- (1) *Lipids: Structure, Physical Properties and Functionality*; Larsson, K., Quinn, P., Sato, K., Tiberg, F., Eds.; The Oily Press: Bridgwater, England, 2006.
- (2) *Physical Properties of Lipids*; Marangoni, A. G., Narine, S. S., Eds.; Marcel Dekker: New York, NY, 2002, pp 63–217.
- (3) Smith, K. W.; Bhaggan, K.; Talbot, G.; van Malssen, K. F. Crystallization of Fats: Influence of Minor Components and Additives. *J. Am. Oil Chem. Soc.* **2011**, *88*, 1085–1101.
- (4) Mazzanti, G.; Li, M.; Marangoni, A. G.; Idziak, S. H. J. Effects of Shear Rate Variation on the Nanostructure of Crystallizing Triglycerides. *Cryst. Growth Des.* **2011**, *11*, 4544–4550.
- (5) Ueno, S.; Ristic, R. I.; Higaki, K.; Sato, K. In situ Studies of Ultrasound-Stimulated Fat Crystallization Using Synchrotron Radiation. *J. Phys. Chem. B* **2003**, *107*, 4927–4935.
- (6) Rousset, P.; Rappaz, M.; Minner, E. Polymorphism and Solidification Kinetics of the Binary System POS–SOS. *J. Am. Oil Chem. Soc.* **1998**, *75*, 857–864.
- (7) Bayés-García, L.; Calvet, T.; Cuevas-Diarte, M. A.; Ueno, S.; Sato, K. In situ synchrotron radiation X-ray diffraction study of crystallization kinetics of polymorphs of 1,3-dioleoyl-2-palmitoyl glycerol (OPO). *CrystEngComm* **2011**, *13*, 3592–3599.
- (8) Bayés-García, L.; Calvet, T.; Cuevas-Diarte, M. A.; Ueno, S.; Sato, K. In situ observation of transformation pathways of polymorphic forms of 1,3-dipalmitoyl-2-oleoyl glycerol (POP) examined with synchrotron radiation X-ray diffraction and DSC. *CrystEngComm* **2013**, *15*, 302–314.
- (9) Foubert, I.; Fredrick, E.; Vereecken, J.; Sichien, M.; Dewettinck, K. Stop-and-return DSC method to study fat crystallization. *Thermochim. Acta* **2008**, *471*, 7–13.
- (10) Campos, R.; Narine, S. S.; Marangoni, A. G. Effect of cooling rate on the structure and mechanical properties of milk fat and lard. *Food Res. Int.* **2002**, *35*, 971–981.
- (11) Svenstrup, G.; Bruggemann, D.; Kristensen, L.; Risbo, J.; Skibsted, L. H. The influence of pretreatment on pork fat crystallization. *Eur. J. Lipid Sci. Technol.* **2005**, *107*, 607–615.
- (12) Campos, R.; Ollivon, M.; Marangoni, A. G. Molecular Composition Dynamics and Structure of Cocoa Butter. *Cryst. Growth Des.* **2010**, *10*, 205–217.

- (13) Chiavaro, E.; Rodríguez-Estrada, M. T.; Bendini, A.; Cerretani, L. Correlation between thermal properties and chemical composition of Italian virgin olive oils. *Eur. J. Lipid Sci. Technol.* **2010**, *112*, 580–592.
- (14) Timms, R. E. Fractional crystallization—the fat modification process for the 21st century. *Eur. J. Lipid Sci. Technol.* **2005**, *107*, 48–57.
- (15) Wheeler, D. H.; Riemschneider, R. W.; Sando, C. E. Preparation, Properties and Thiocyanogen Absorption of Triolein and Trilinolein. *J. Biol. Chem.* **1940**, *132*, 687–699.
- (16) Ferguson, R. H.; Lutton, E. S. The Polymorphism of Triolein. *J. Am. Chem. Soc.* **1947**, *69*, 1445–1449.
- (17) Hagemann, J. W.; Tallent, W. H.; Kolb, K. E. Differential Scanning Calorimetry of Single Acid Triglycerides: Effect of Chain Length and Unsaturation. *J. Am. Oil Chem. Soc.* **1972**, *49* (2), 118–123.
- (18) Sato, K.; Ueno, S. In *Bailey's Industrial Oil and Fat Products*; Shahidi, F., Ed.; John Wiley & Sons Inc.: Hoboken, NJ, 2005; Vol. 1, pp 77–120.
- (19) Akita, A.; Kawaguchi, T.; Kaneko, F. Structural Study on Polymorphism of Cis-Unsaturated Triacylglycerol: Triolein. *J. Phys. Chem. B* **2006**, *110*, 4346–4353.
- (20) Mortimer, R. G. *Mathematics for Physical Chemistry*; Elsevier Academic Press: San Diego, CA, 2005, 326.
- (21) Chapman, D. The Polymorphism of Glycerides. *Chem. Rev.* **1962**, *62* (5), 433–456.
- (22) Ostwald, W. Studien über die Bildung und Umwandlung fester Körper. *Z. Phys. Chem.* **1897**, *22*, 289–330.
- (23) Kodali, D. R.; Atkinson, D.; Small, D. M. Polymorphic behavior of 1,2-dipalmitoyl-3-lauroyl(PP12)- and 3-myristoyl(PP14)-*sn*-glycerols. *J. Lipid Res.* **1990**, *31*, 1853–1864.
- (24) Minato, A.; Ueno, S.; Smith, K.; Amemiya, Y.; Sato, K. Thermodynamic and Kinetic Study on Phase Behavior of Binary Mixtures of POP and PPO Forming Molecular Compound Systems. *J. Phys. Chem. B* **1997**, *101*, 3498–3505.
- (25) Takeuchi, M.; Ueno, S.; Sato, K. Crystallization kinetics of polymorphic forms of a molecular compound constructed by SOS (1,3-distearoyl-2-oleoyl-*sn*-glycerol) and SSO (1,2-distearoyl-3-oleoyl-*rac*-glycerol). *Food Res. Int.* **2002**, *35*, 919–926.
- (26) Zhang, L.; Ueno, S.; Miura, S.; Sato, K. Binary Phase Behavior of 1,3-Dipalmitoyl-2-oleoyl-*sn*-glycerol and 1,2-Dioleoyl-3-palmitoyl-*rac*-glycerol. *J. Amer. Oil Chem. Soc.* **2007**, *84*, 219–227.
- (27) Zhang, L.; Ueno, S.; Sato, K.; Adlof, R. O.; List, G. R. Thermal and structural properties of binary mixtures of 1,3-distearoyl-2-oleoyl-glycerol (SOS) and 1,2-dioleoyl-3-stearoyl-*sn*-glycerol (*sn*-OOS). *J. Therm. Anal. Calorim.* **2009**, *98*, 105–111.
- (28) Small, D. M. Lateral chain packing in lipids and membranes. *J. Lipid Res.* **1984**, *25*, 1490–1500.
- (29) Jiang, J.; Zhuralev, E.; Huang, Z.; Wei, L.; Shan, M.; Xue, G.; Zhou, D.; Schick, C.; Jian, W. A transient polymorph transition of 4-cyano-4'-octyloxybiphenyl (8CB) revealed by ultrafast differential scanning calorimetry (UFDSC). *Soft Matter* **2013**, *9*, 1488–1491.